JCI The Journal of Clinical Investigation

microRNA-206 promotes skeletal muscle regeneration and delays progression of Duchenne muscular dystrophy in mice

Ning Liu, … , Rhonda Bassel-Duby, Eric N. Olson

J Clin Invest. 2012;122(6):2054-2065. https://doi.org/10.1172/JCI62656.

Research Article **Muscle biology**

Skeletal muscle injury activates adult myogenic stem cells, known as satellite cells, to initiate proliferation and differentiation to regenerate new muscle fibers. The skeletal muscle–specific microRNA miR-206 is upregulated in satellite cells following muscle injury, but its role in muscle regeneration has not been defined. Here, we show that miR-206 promotes skeletal muscle regeneration in response to injury. Genetic deletion of miR-206 in mice substantially delayed regeneration induced by cardiotoxin injury. Furthermore, loss of miR-206 accelerated and exacerbated the dystrophic phenotype in a mouse model of Duchenne muscular dystrophy. We found that miR-206 acts to promote satellite cell differentiation and fusion into muscle fibers through suppressing a collection of negative regulators of myogenesis. Our findings reveal an essential role for miR-206 in satellite cell differentiation during skeletal muscle regeneration and indicate that miR-206 slows progression of Duchenne muscular dystrophy.

microRNA-206 promotes skeletal muscle regeneration and delays progression of Duchenne muscular dystrophy in mice

Ning Liu,[1] Andrew H. Williams,[1] Johanna M. Maxeiner,[1] Svetlana Bezprozvannaya,[1] John M. Shelton,[2] James A. Richardson,[1,3] Rhonda Bassel-Duby,[1] and Eric N. Olson[1]

[1]Department of Molecular Biology, [2]Department of Internal Medicine, and [3]Department of Pathology, University of Texas Southwestern Medical Center, Dallas, Texas, USA.

Skeletal muscle injury activates adult myogenic stem cells, known as satellite cells, to initiate proliferation and differentiation to regenerate new muscle fibers. The skeletal muscle–specific microRNA miR-206 is upregulated in satellite cells following muscle injury, but its role in muscle regeneration has not been defined. Here, we show that miR-206 promotes skeletal muscle regeneration in response to injury. Genetic deletion of miR-206 in mice substantially delayed regeneration induced by cardiotoxin injury. Furthermore, loss of miR-206 accelerated and exacerbated the dystrophic phenotype in a mouse model of Duchenne muscular dystrophy. We found that miR-206 acts to promote satellite cell differentiation and fusion into muscle fibers through suppressing a collection of negative regulators of myogenesis. Our findings reveal an essential role for miR-206 in satellite cell differentiation during skeletal muscle regeneration and indicate that miR-206 slows progression of Duchenne muscular dystrophy.

Introduction

Adult skeletal muscle can regenerate in response to exercise, injury, and disease. Skeletal muscle regeneration relies on a small population of stem cells, known as satellite cells (SCs), which reside beneath the basal lamina of myofibers (1, 2). SCs are normally quiescent, but, in response to stress or injury, become activated to proliferate, differentiate, and fuse into multinucleated myotubes (3–6). Activated SCs also undergo asymmetric division, generating progeny that replenish the pool of quiescent SCs (5). Abnormalities in SC specification, proliferation, or differentiation result in skeletal muscle dysfunction during aging and can promote muscle disease (7).

The paired-box transcription factor Pax7 is a specific marker for quiescent and activated SCs and is downregulated when SCs differentiate into myotubes (5, 8). Pax7 activates expression of the myogenic regulatory factors Myf5 and MyoD in activated SCs and proliferating myoblasts, which in turn drive the myogenic differentiation program (9). Although stem/progenitor cells from other cell origins have also been reported to contribute to regeneration of new myofibers, SC ablation experiments have clearly demonstrated that Pax7-expressing SCs are indispensable for adult skeletal muscle regeneration (10–13).

Duchenne muscular dystrophy (DMD), the most common and severe form of muscular dystrophy, is caused by mutations in the dystrophin gene on the X chromosome (14, 15). Loss of the subsarcolemmal protein dystrophin in DMD patients causes sensitivity of myofibers to mechanical damage, leading to SC activation and myofiber regeneration (16). However, the unsustainable activation of SCs in DMD patients ultimately results in severe muscle wasting, infiltration of adipocytes, inflammation, and eventual paralysis and death (17). *Mdx* mice, which harbor a premature termination codon in the dystrophin gene, are the most commonly used mouse model of muscular dystrophy (18). Intriguingly, despite sharing the same genetic defects as DMD patients, *mdx* mice display a relatively mild and slowly progressive dystrophic phenotype, marked by chronic SC activation and regeneration. The relatively mild phenotype of *mdx* mice has been attributed to the increased regenerative capacity of mouse SCs due to the longer telomeres in mice relative to humans (19). Understanding the mechanisms of DMD pathology remains an important challenge in the quest to develop efficacious therapies for DMD patients.

microRNAs (miRNAs) are a class of small noncoding RNAs that inhibit gene expression via Watson-Crick base pairing between the miRNA "seed" region and sequences located predominantly in the 3′ UTRs of target mRNAs (20). Changes in miRNA expression are associated with various skeletal muscle disorders, including muscular dystrophies (21, 22). The skeletal muscle–specific miRNA miR-206 is required for efficient regeneration of neuromuscular synapses after acute nerve injury, and the absence of miR-206 accelerates disease progression of amyotrophic lateral sclerosis (ALS) in mice (23). miR-206 is upregulated during skeletal muscle regeneration and has been reported to repress proliferation and promote differentiation of SCs in vitro (24, 25). However, the functions of miR-206 in skeletal muscle regeneration in vivo have not been determined.

In the present study, we show that mice lacking miR-206 have inefficient skeletal muscle regeneration in response to cardiotoxin (CTX) injury. Loss of miR-206 also results in acceleration and exacerbation of muscle dysfunction in *mdx* mice. The inefficient skeletal muscle regeneration in mice lacking miR-206 results from impaired differentiation of SCs and correlates with the dysregulation of a collection of negative regulators of myogenesis. Our findings reveal an important role for miR-206 as a modulator of DMD and a potential target for therapeutic intervention in this disease.

Authorship note: Ning Liu and Andrew H. Williams contributed equally to this work.

Conflict of interest: Eric N. Olson is cofounder of miRagen Therapeutics, a company focused on developing miRNA-based therapies for cardiovascular disease.

Citation for this article: *J Clin Invest.* 2012;122(6):2054–2065. doi:10.1172/JCI62656.

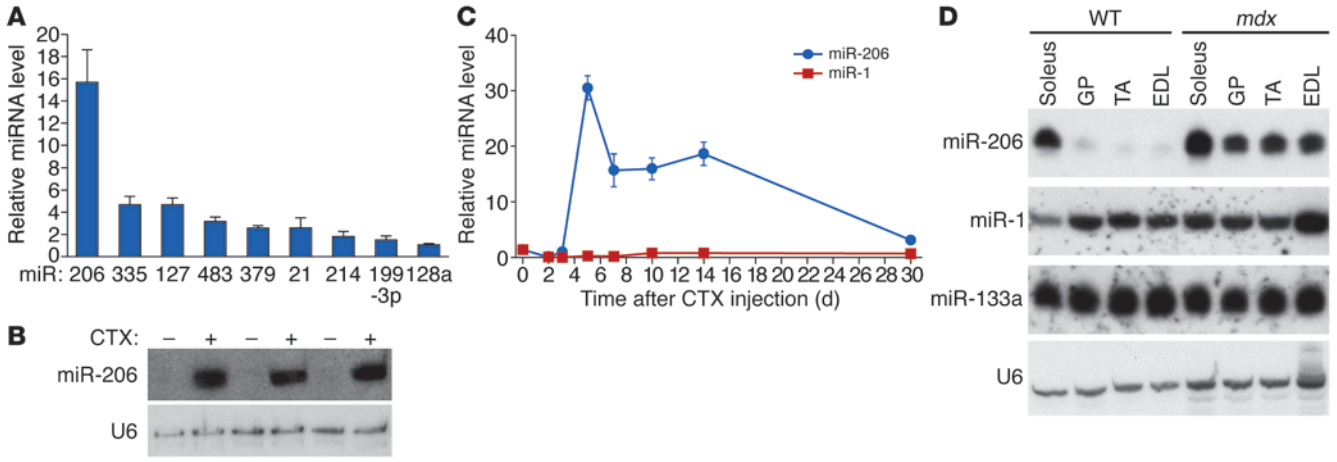

Figure 1

miR-206 is upregulated during skeletal muscle regeneration and in *mdx* mice. (**A**) Real-time RT-PCR shows upregulated miRNAs in TA muscle 7 days after CTX injury. *y* axis represents miRNA expression in injured muscle (CTX) relative to control muscle. $n = 6$ for each group. (**B**) Northern blot for miR-206 in control (–) and CTX-injured (+) TA muscle on day 7 after injury. U6 is a loading control. (**C**) Real-time RT-PCR of miR-1 and miR-206 expression in TA muscle from day 2 to day 30 after CTX injury. (**D**) Northern blot of miR-206, miR-1, miR-133a, and U6 in various muscles of WT and *mdx* mice at 3 months of age. GP, gastrocnemius and plantaris; EDL, extensor digitorum longus. Data are presented as mean ± SEM.

Results

Upregulation of miR-206 during skeletal muscle regeneration. In an effort to identify miRNAs involved in skeletal muscle regeneration, we induced skeletal muscle injury and regeneration in mice by injecting CTX in the tibialis anterior (TA) muscle and compared the miRNA expression profile 7 days after CTX injection with that of untreated control TA muscle. Microarray analysis identified a number of miRNAs that were dysregulated upon CTX injection (Figure 1A and Supplemental Figure 1, A and B; supplemental material available online with this article; doi:10.1172/JCI62656DS1). miR-206 was the most dramatically upregulated miRNA in CTX-injured TA muscle on day 7, as confirmed by real-time RT-PCR and Northern blot analysis (Figure 1, A and B). miR-206 continued to be strongly expressed throughout the course of muscle regeneration (Figure 1C). miR-206 is generated from a bicistronic transcript that also includes miR-133b (23). Two other homologous pairs of muscle-specific miRNAs, miR-1-1/133a-2 and miR-1-2/133a-1, are expressed from separate chromosomes (26). miR-133b was also strongly upregulated following CTX injection, whereas the expression of miR-1, which shares high sequence homology with miR-206, was modestly downregulated (Figure 1C and Supplemental Figure 1C).

We also examined the regulation of miR-206 during the progression of muscular dystrophy in *mdx* mice. At 2 weeks of age, prior to the onset of muscle damage, miR-206 was expressed in *mdx* muscle at levels comparable to those in WT muscle (Supplemental Figure 2A), whereas by 4 weeks of age, after the onset of necrosis and myofiber degeneration, miR-206 was upregulated in various muscles of *mdx* mice (Figure 1D and Supplemental Figure 2). Consistent with these findings, miR-206 expression has been reported to be enriched in newly formed myofibers with centralized nuclei in *mdx* TA muscle, but not in intact fibers (24, 27). These data indicate that miR-206 expression is dramatically upregulated in pharmacologic and genetic models of skeletal muscle regeneration and muscular dystrophy.

Delayed skeletal muscle regeneration in mice lacking miR-206. In light of the strong upregulation of miR-206 expression during skeletal muscle regeneration and its enrichment in activated SCs (25), we injected WT and miR-206–KO mice with CTX and analyzed myofiber regeneration at various time points. miR-206–KO mice do not exhibit apparent histological or functional muscle defects under normal conditions (23). Three days following CTX injection, WT and miR-206–KO mice exhibited extensive myofiber degeneration and accumulation of small mononucleated cells at the site of injury, which included proliferating myoblasts, macrophages, and neutrophils (Figure 2A). Seven days following CTX injection, most damaged myofibers in WT mice were cleared and replaced by newly formed myofibers containing centralized nuclei (Figure 2A). In contrast, in miR-206–KO mice, abundant inflammatory cells and damaged myofibers were still present 7 days following CTX injection. On days 14 and 30 following CTX injection, muscle architecture was largely restored in both WT and miR-206–KO mice, indicating that the absence of miR-206 delays but does not completely prevent regeneration (Figure 2A). The delayed regeneration response of miR-206–KO muscle was further revealed by extensive mineralization 14 and 30 days following CTX injection, which resulted from accumulation of damaged muscle fibers (Figure 2A). Oil red O staining also revealed slightly increased fatty infiltration in miR-206–KO mice 30 days following CTX injection (Supplemental Figure 3C). Loss of miR-206 does not affect capillary density of TA muscle 30 days after CTX injection, as assessed by immunostaining for platelet endothelial cell adhesion molecule (PECAM1) staining (Supplemental Figure 3D), indicating that angiogenesis after CTX injury is not affected in miR-206–KO mice.

Whereas there was no significant difference in fiber size between WT and miR-206–KO mice under normal conditions (Supplemental Figure 3, A and B), regenerated myofibers in miR-206–KO mice were significantly smaller than those of WT mice (Figure 2B). Immunostaining for the intermediate filament protein desmin, which is highly expressed in immature muscle fibers during fetal

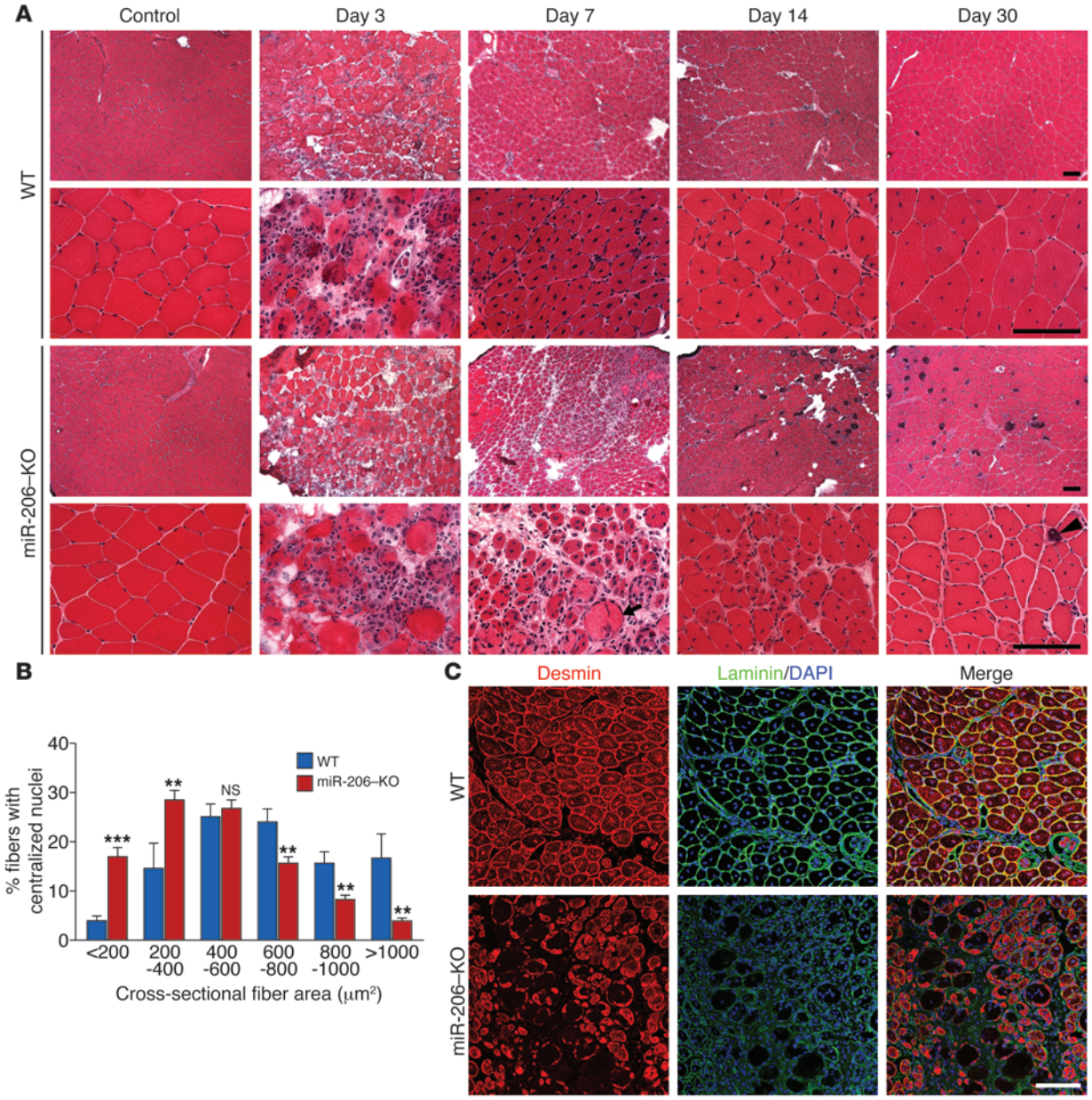

Figure 2

Delayed regeneration in miR-206–KO mice after CTX injury. (**A**) H&E staining of transverse sections of WT and miR-206–KO TA muscles at days 3, 7, 14, and 30 after CTX injury. Arrow indicates degenerating myofibers in miR-206–KO muscle at day 7. Arrowhead points to mineralization in myofibers in miR-206–KO muscle at day 30 after injury. Scale bars: 100 μm. (**B**) Cross-sectional areas of regenerated myofibers in WT and miR-206-KO TA muscle 7 days after CTX injury were measured by ImageJ based on laminin staining of CTX-injured TA muscle sections. Only myofibers that contained centralized nuclei were counted. Five mice of each genotype were counted. ***$P < 0.001$; **$P < 0.01$. Data are presented as mean ± SEM. (**C**) Immunostaining for desmin and laminin on WT and miR-206–KO TA muscles at day 7 after injury. Scale bar: 100 μm.

life and regeneration (28, 29), showed that desmin was strongly expressed in most myofibers in WT mice 7 days following CTX injection (Figure 2C). However, in miR-206–KO mice, desmin expression was absent in many myofibers, and desmin-positive fibers that were present displayed heterogeneity in size, confirming the impairment in regeneration of miR-206–KO muscle (Figure 2C).

Loss of miR-206 exacerbates the dystrophic phenotype in mdx mice. To investigate the potential involvement of miR-206 in muscular dystrophy, we generated *mdx* mice lacking expression of miR-206 and compared the morphology of quadriceps and diaphragm muscles of *mdx* and miR-206–KO;*mdx* mice at different ages. Mice used in these studies were of 129SvEv-C57BL/6 mixed background. Absence of miR-206 expression was confirmed by Northern blot analysis (Supplemental Figure 4). At 2 weeks of age, the quadriceps muscle in *mdx* mice showed a largely normal morphology (Supplemental Figure 5A). Small regenerating fibers and associated mononucleated cells were only occasionally observed in a minor subset of miR-206–KO;*mdx* mice (Supplemental Figure 5A). Strikingly, how-

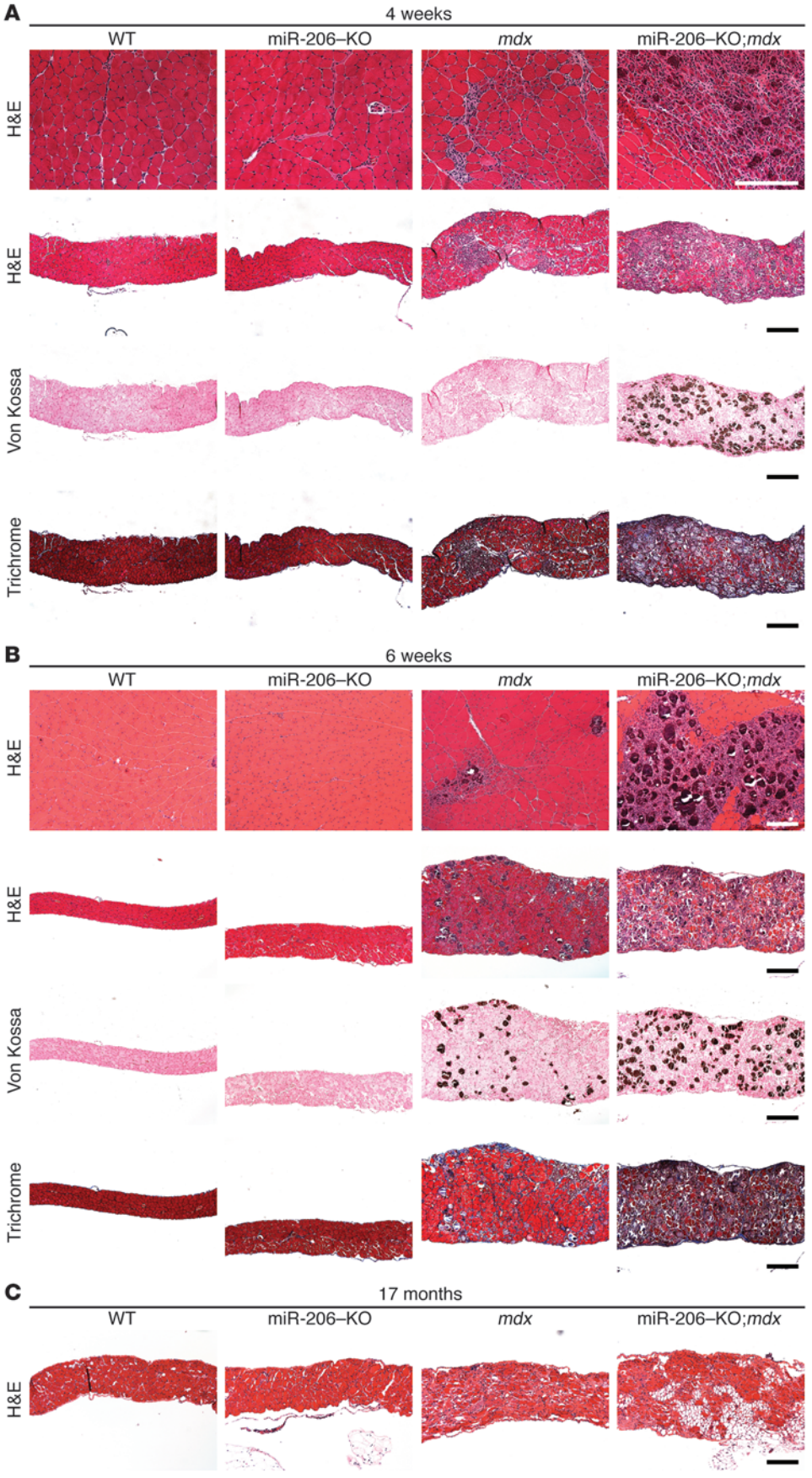

Figure 3

Loss of miR-206 exacerbates the dystrophic phenotype in *mdx* mice. (**A**) H&E staining of quadriceps and diaphragm muscle of WT, miR-206–KO, *mdx*, and miR-206–KO;*mdx* mice at 4 weeks of age. Upper 2 rows: H&E staining of quadriceps and diaphragm muscles, respectively. Lower 2 rows: von Kossa staining and Masson's trichrome staining of diaphragm muscle showing mineralization and fibrosis in diaphragm muscle fibers. Scale bars: 200 μm. (**B**) H&E staining of quadriceps and diaphragm muscle of WT, miR-206–KO, *mdx*, and miR-206–KO;*mdx* mice at 6 weeks of age. Upper 2 rows: H&E staining of quadriceps and diaphragm muscles, respectively. Lower 2 rows: von Kossa staining and Masson's trichrome staining of diaphragm muscle showing mineralization and fibrosis in diaphragm muscle fibers. Scale bars: 100 μm. (**C**) H&E staining of the diaphragm muscle in WT, miR-206–KO;*mdx*, and miR-206–KO;*mdx* mice at 17 months of age. Infiltration of fat tissue was apparent in the diaphragm muscle of miR-206–KO;*mdx* mice. Scale bar: 100 μm.

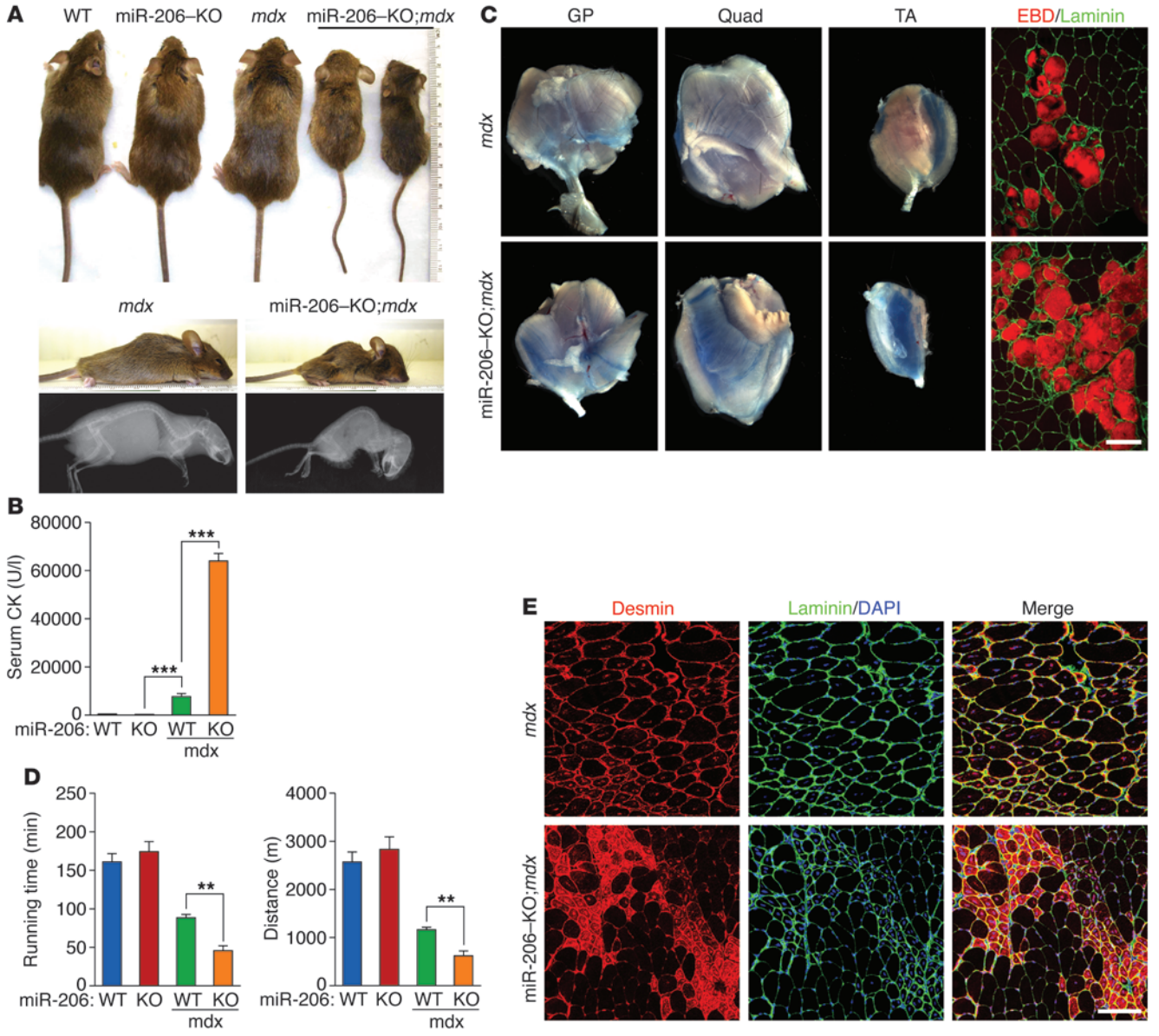

Figure 4

Analysis of the more severe dystrophic phenotype of miR-206–KO;*mdx* mice. (**A**) WT, miR-206–KO, *mdx*, and miR-206–KO;*mdx* mice at 6 weeks of age. miR-206–KO;*mdx* mice are runted with kyphosis compared with *mdx* mice. Kyphosis was revealed by x-ray in miR-206–KO;*mdx* mice. (**B**) Serum CK levels of WT, miR-206–KO, *mdx*, and miR-206–KO;*mdx* mice at 4 weeks of age. 6 mice were analyzed from each genotype. ***$P < 0.001$. (**C**) Results of Evans blue dye (EBD) uptake of GP muscle, quadriceps (quad), and TA muscles of *mdx* and miR-206;*mdx* mice. Immunostaining with laminin (green) is shown in the right column. Evans blue dye is detected as a red signal under fluorescence microscopy. Scale bar: 100 μm. (**D**) Ten-week-old WT, miR-206–KO, *mdx*, and miR-206–KO;*mdx* mice were subjected to forced downhill running on a treadmill. Muscle performance was measured as time to exhaustion. Left panel: total running time. Right panel: total running distance. Six mice were analyzed from each genotype. **$P < 0.01$. (**E**) Immunostaining for desmin and laminin on quadriceps muscle of *mdx* and miR-206–KO;*mdx* mice at 6 weeks of age. Scale bar: 100 μm. Data are presented as mean ± SEM.

ever, by 4 weeks of age, nearly all miR-206–KO;*mdx* mice showed severe dystrophic phenotypes compared with *mdx* mice. We observed massive accumulation of small regenerating fibers and inflammatory cells in miR-206–KO;*mdx* quadriceps muscle (Figure 3A). Similarly, the diaphragm of miR-206–KO;*mdx* mice showed extensive fiber damage and degeneration, with calcium deposition, mineralization, and fibrosis (Figure 3A). The dystrophic phenotype became more apparent at 6 weeks of age, when approximately 17% of miR-206–KO;*mdx* mice became severely runted, showed kyphosis, and died (Figure 4A). In contrast, only 5% of *mdx* mice died at this age (Figure 4A). Histological analysis revealed especially severe muscle degeneration, mineralization, and fibrosis in miR-206–KO;*mdx* mice compared with *mdx* mice (Figure 3B).

Although miR-206–KO;*mdx* mice that survived beyond 8 weeks showed a life span similar to that of *mdx* mice, these mice generally had worse dystrophic phenotypes than *mdx* mice. At advanced ages

Table 1
Genes upregulated in miR-206–KO;*mdx* mice compared with *mdx* mice

Category	Gene symbol	Fold change (miR-206–KO; *mdx/mdx*)	Gene name
Muscle regeneration	*Myh3*	3.2	Mus musculus myosin, heavy polypeptide 3, skeletal muscle, embryonic
	Myh8	2.93	Mus musculus myosin, heavy polypeptide 8, skeletal muscle, perinatal
	Myl14	2.2	Mus musculus myosin, light polypeptide 4
	Tnni1	2.52	Mus musculus troponin T1, skeletal, slow
Chemokines, cytokines, interleukins, and receptors	*Ccl7*	3.7	Mus musculus chemokine (C-C motif) ligand 7
	Ccl9	3.2	Mus musculus chemokine (C-C motif) ligand 9
	Cxcl4	2.33	Mus musculus chemokine (C-X-C motif) ligand 4, mRNA
	Igf-2	2.0	Mus musculus insulin-like growth factor 2
	Lyzs	1.9	Mus musculus lysozyme, mRNA
	Il1rl1	1.7	Mus musculus interleukin 1 receptor-like 1, transcript variant 2, mRNA
ECM and ECM processing	*TIMP-1*	1.9	Mus musculus tissue inhibitor of metalloproteinase 1, transcript variant 2, mRNA
Angiogenesis and vascular response	*ApoE*	1.9	Mus musculus ApoE, mRNA
Cytoskeleton	*Tubb2b*	1.8	Mus musculus tubulin, β 2b, mRNA
	Coro1a	2.0	Mus musculus coronin, actin binding protein 1A, mRNA
	Acta2	1.7	Mus musculus actin, α 2, smooth muscle, aorta, mRNA

(>17 months), miR-206–KO;*mdx* mice showed debilitating muscle wasting and infiltration of fat in the diaphragm muscle compared with *mdx* mice (Figure 3C). In contrast with other muscle groups, the soleus muscle of miR-206–KO;*mdx* mice was indistinguishable from that of *mdx* mice (data not shown), which likely reflects the resistance of slow twitch myofibers in the soleus muscle to dystrophy. There were no apparent cardiac abnormalities in miR-206–KO;*mdx* mice at 3 months of age as measured by echocardiography and histological analysis (Supplemental Figure 5, C and D).

To further characterize the dystrophic phenotype of miR-206–KO;*mdx* mice, we measured the levels of serum creatine kinase (CK), an indicator of skeletal muscle damage, and diagnostic marker for DMD patients (30). At 4 weeks of age, serum CK levels of *mdx* mice were elevated 14-fold compared with those of WT and miR-206–KO mice (Figure 4B). Intriguingly, serum CK levels of miR-206–KO;*mdx* mice were more than 8-fold higher than those of *mdx* mice (Figure 4B). At 5 months of age, the difference in serum CK levels between *mdx* and miR-206–KO;*mdx* mice became less dramatic. However, miR-206–KO;*mdx* mice still showed an approximately 1.5-fold increase in serum CK levels compared with *mdx* mice (Supplemental Figure 5B). Myofiber membrane permeability, monitored by Evans blue dye uptake, was also exacerbated in miR-206–KO;*mdx* mice (Figure 4C).

To assess muscle functionality and performance, we subjected mice to a downhill treadmill exercise paradigm and measured the running time and distance to exhaustion. At 3 months of age, *mdx* mice ran for a significantly shorter time than WT or miR-206–KO mice (Figure 4D). Muscle performance in miR-206–KO;*mdx* mice was further decreased compared with *mdx* mice, indicative of severe muscle injury and dysfunction (Figure 4D). These findings support the histological data and further indicate that the absence of miR-206 sensitizes mice to dystrophic abnormalities.

Immunostaining of 6-week-old muscle sections revealed strong accumulation of desmin in small regenerating myofibers that contained centralized nuclei in miR-206–KO;*mdx* mice (Figure 4E). In contrast, regenerating fibers in *mdx* mice displayed weaker desmin signal and were larger (Figure 4E), indicating that the regenerating fibers in miR-206–KO;*mdx* mice were less mature than in *mdx* mice. Microarray analysis on muscles from *mdx* and miR-206–KO;*mdx* mice also revealed upregulation of embryonic muscle genes as well as inflammatory genes, confirming the delayed regeneration in miR-206–KO;*mdx* mice (Table 1). Taken together, these data support the conclusion that loss of miR-206 in the *mdx* background causes a delay in regeneration and maturation of myofibers to replace damaged fibers, which contributes to the more severe dystrophic phenotype in compound mutant mice.

miR-206 is required for the efficient regeneration of neuromuscular junctions (NMJs) following nerve injury in mice (23). *mdx* mice also have structural abnormalities in NMJs, although the functional significance of this observation is unknown (31). To determine whether the more severe dystrophic phenotype of miR-206–KO;*mdx* mice was due to innervation defects of NMJs, we compared the innervation of *mdx* and miR-206–KO;*mdx* mice using markers for the postsynaptic membrane (α-bungarotoxin [BTX]) and presynaptic nerve terminals (synaptophysin) (32). We observed no differences in the number of synapses or the innervation of NMJs between *mdx* and miR-206–KO;*mdx* mice (Supplemental Figure 5B). Thus, we conclude that the severe dystrophic phenotypes observed in miR-206–KO;*mdx* mice are due to a function of miR-206 independent of motor innervation.

miR-206 regulates SC differentiation. To directly examine the influence of miR-206 on SC function in vivo, we isolated activated SCs from WT and miR-206–KO mice by FACS (refs. 5, 7, and Supplemental Figure 6, A and B). We found no significant difference in the fraction of SCs between WT and miR-206–KO mice 3 days following CTX injury (Supplemental Figure 6A). We confirmed the expression of miR-206 in cultured SCs, but not in the non-SC population by Northern blot analysis (Supplemental Figure 6C). We also analyzed the proliferation of SCs isolated from WT and miR-206–KO mice, but found no differences in the proliferation rates of these cells in culture (Supplemental Figure 7, A and B). These findings contrast with a previous report that miR-206 represses SC proliferation based on overexpression or oligonucleotide-mediated inhibition of miR-206 in vitro (25).

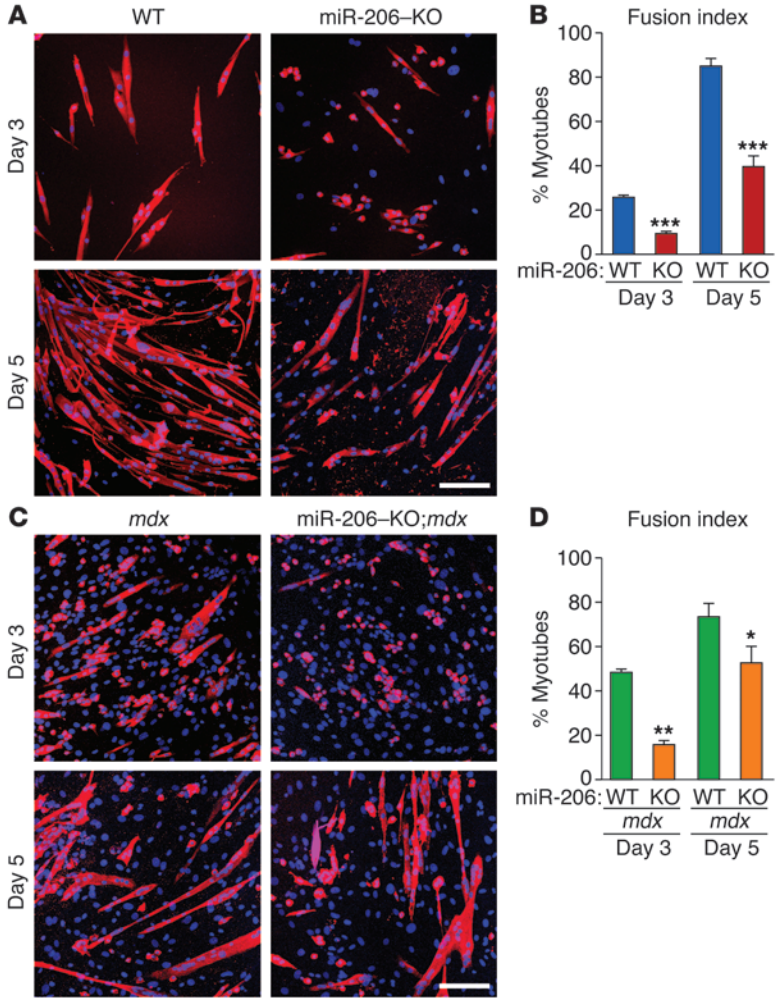

Figure 5

miR-206 regulates SC differentiation. (**A**) WT and miR-206–KO SCs were cultured in differentiation medium for 3 and 5 days, and myogenic differentiation was determined by immunostaining against MHC. Scale bar: 100 μm. (**B**) Measurement of fusion index is determined by percentage of MHC-positive cells that contained 2 or more nuclei among the total MHC-positive cells. ***$P < 0.001$. (**C**) *mdx* and miR-206–KO;*mdx* SCs were cultured in differentiation medium for 3 and 5 days, and myogenic differentiation was determined by immunostaining against MHC. Scale bar: 100 μm. (**D**) Measurement of fusion index is determined by percentage of MHC-positive cells that contained 2 or more nuclei among the total MHC-positive cells. *$P < 0.05$; **$P < 0.01$. Data are presented as mean ± SEM.

To investigate whether miR-206 modulates SC differentiation, we isolated WT and miR-206–KO SCs by FACS and assessed their ability to differentiate and form myotubes at different time points. Three days after induction of differentiation, most WT SCs became elongated and fused and expressed the differentiation marker myosin heavy chain (MHC) (Figure 5, A and B). In contrast, elongation, fusion, and MHC expression were delayed in miR-206–KO SCs (Figure 5, A and B). After 5 days in differentiation medium, most WT SCs had fused to form myotubes, whereas only 40% of miR-206–KO cells underwent fusion (Figure 5, A and B). We also analyzed the differentiation of SCs from *mdx* and miR-206–KO;*mdx* mice. Similar to the miR-206–KO SCs, we observed delayed fusion of miR-206–KO; *mdx* SCs compared with *mdx* SCs (Figure 5, C and D). These results indicate that the absence of miR-206 causes a cell-autonomous delay in SC differentiation. They are also consistent with the previous finding that loss of miR-206 delayed rather than completely blocked regeneration upon CTX injury (Figure 2A).

miR-206 targets regulators of SC differentiation. miR-206 has been reported to directly repress Pax7 expression during SC proliferation and differentiation in vitro (25, 27). While *Pax7* mRNA levels were upregulated approximately 1.7-fold, Pax7 protein levels were unchanged in miR-206–KO SCs compared with WT under growth conditions (Figure 6, A and B). *Pax7* mRNA and protein are downregulated during differentiation of WT SCs (8). Interestingly, this repression was attenuated in miR-206–KO cells under the same differentiation conditions, such that Pax7 protein was still detectable in miR-206–KO SCs, but not in WT cells 5 days after differentiation (Figure 6, A and B). Using luciferase reporter assays, we found that miR-206 could directly repress *Pax7* mRNA translation through interactions with 4 binding sites in the 3′ UTR (Supplemental Figure 8A). These results indicate that miR-206 regulates Pax7 expression during SC differentiation.

In addition to *Pax7*, we identified and confirmed several other miR-206 target genes with functions in myoblast and SC differentiation that were upregulated in miR-206–KO SCs. *Notch3* mRNA and protein expression was upregulated in miR-206–KO SCs, with the upregulation being more pronounced in miR-206–KO SC–derived myotubes (Figure 6, A and B). Notch3 functions as an inhibitor of MyoD-induced myogenesis (33). Thus, its upregulation would be inhibitory to the differentiation process. We identified 3 miR-206–binding sites within the 3′ UTR of *Notch3* mRNA, 2 of which are evolutionarily conserved (Figure 6C). In luciferase assays, miR-206 repressed a luciferase reporter gene linked to the Notch3 3′ UTR, whereas mutation in all 3 predicted miR-206–binding sites abrogated this repression (Figure 6C). In addition, we identified IGF-binding protein 5 (Igfbp5) as a miR-206 target gene. Igfbp5 is a secreted factor that has previously been shown to inhibit skeletal muscle differentiation through IGF-dependent mechanisms (34–36). IGFBP5 protein expression was upregulated in miR-206–KO SCs and miR-206 SC–derived myotubes compared with WT cells (Figure 6, A and B). The 3′ UTR of *Igfbp5* mRNA contains one evolutionarily conserved miR-206–binding site (Figure 6D). In luciferase assays, miR-206 repressed a luciferase reporter gene linked to the Igfbp5 3′ UTR, and mutations in the predicted miR-206–binding site abrogated the repression, confirming Igfbp5 as a target of miR-206 (Figure 6D). In addition, we also confirmed upregulation of Gja1 (connexin 43) in miR-206–KO SCs upon differentiation (Supplemental Figure 8B), although the potential function of connexin 43 in myogenesis remains unknown (37). Previously published miR-206 target genes, such as utrophin and myostatin, did not show differences in their expression in miR-206–KO SCs compared with WT cells (Supplemental Figure 8C). In addition, expression of Integrin α7 (*Itga7*) and VEGF was not changed in miR-206–KO SCs (Supplemental Figure 8C). In

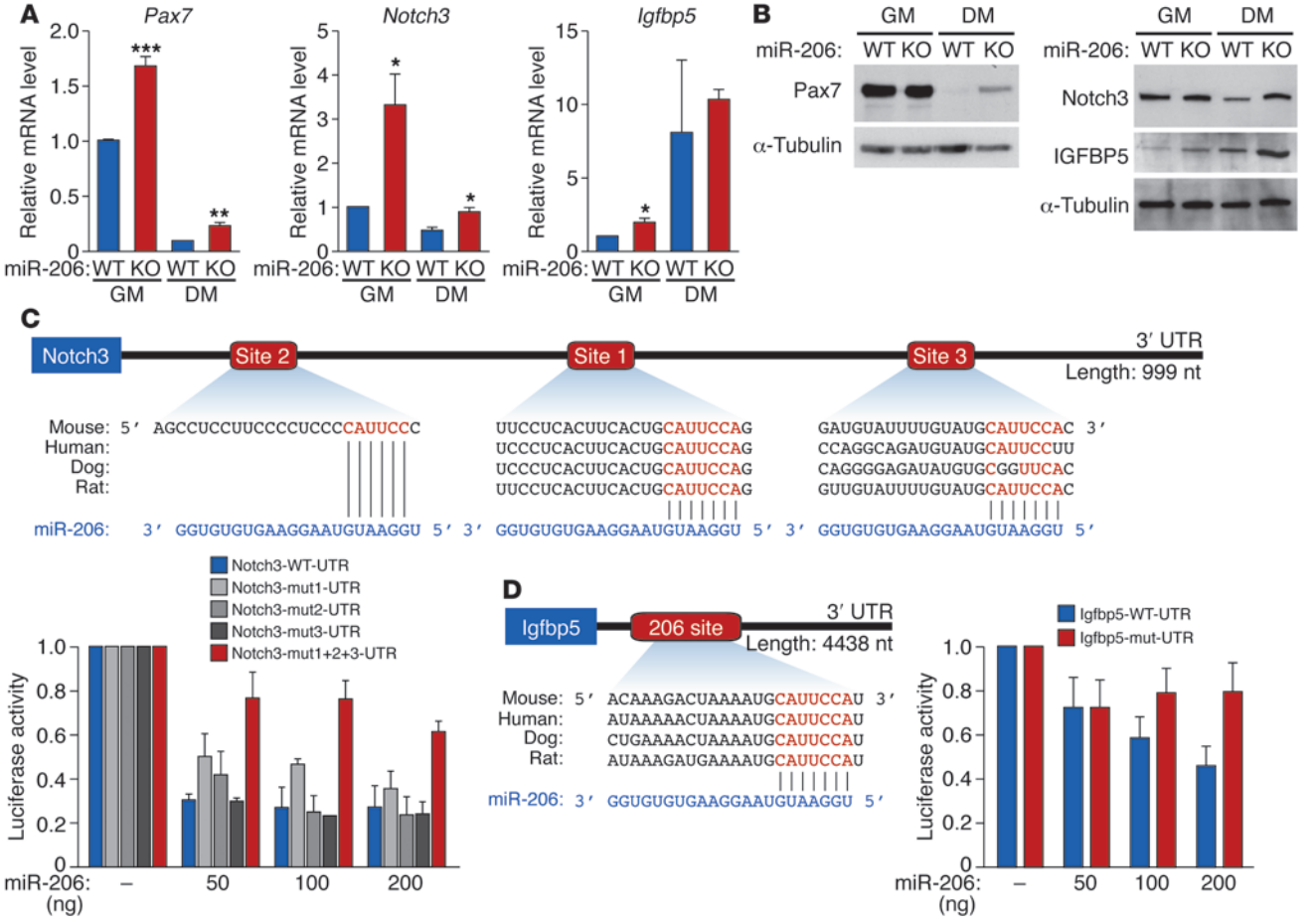

Figure 6

miR-206 regulates expression of target genes involved in SC proliferation and differentiation. (**A**) Real-time RT-PCR reveals expression of *Pax7*, *Notch3*, and *Igfbp5* mRNA in WT and miR-206–KO SCs. GM, cells were cultured in growth medium; DM, cells were cultured in differentiation medium for 5 days. **P* < 0.05; ***P* < 0.01; ****P* < 0.001. (**B**) Western blot analysis reveals protein levels of target genes in WT and miR-206-KO SCs. α-Tubulin was detected as a loading control. (**C**) miR-206 directly represses WT Notch3 3′ UTR in luciferase assay, and the repression is abolished when all 3 miR-206–binding sites in Notch3 3′ UTR are mutated. Conserved miR-206–binding sites in Notch3 3′ UTR are also shown in red. (**D**) miR-206 directly represses WT Igfbp5 3′ UTR in luciferase assay, and the repression is abolished when the miR-206 binding site is mutated. Conserved miR-206–binding site in Igfbp5 3′ UTR is also shown in red. Data are presented as mean ± SEM.

summary, loss of miR-206 results in upregulation of Pax7, Notch3, and Igfbp5 in differentiating SCs compared with WT cells, implying that repression of these inhibitors of myogenesis accounts, at least in part, for the stimulatory influence of miR-206 on SC differentiation and skeletal muscle regeneration.

Discussion

The results of this study reveal an important role of miR-206 in promoting efficient skeletal muscle regeneration in response to injury or disease. Whereas mice lacking miR-206 do not exhibit overt abnormalities at baseline, the absence of miR-206 in mice results in a delay in skeletal muscle regeneration in response to CTX injury and an exacerbated dystrophic phenotype in *mdx* mice. These data identify miR-206 as an important modifier of muscular dystrophy disease progression. Our results extend recent findings that miRNAs frequently function as "fine-tuners" of cellular phenotypes under conditions of tissue homeostasis, whereas their functions become magnified under conditions of injury or stress.

miR-206 and skeletal muscle regeneration. Skeletal muscle regeneration in response to injury involves a highly orchestrated series of events accompanied by necrosis and activation of an inflammatory response, leading to myofiber degeneration and the activation of myogenic cells to proliferate, differentiate, and fuse to generate new myofibers (2). miR-206 is expressed at a low level in adult myofibers, but is highly enriched in newly regenerated myofibers during muscle regeneration. The upregulation of miR-206 following injury correlates with the time in which proliferating myoblasts initiate differentiation into mature myotubes and upregulate the myogenic transcription factors MyoD and myogenin, which directly activate miR-206 expression (23, 38). Indeed, miR-206 is strongly expressed in activated SCs, in which MyoD expression is already turned on (Supplemental Figure 6C).

It has been reported that injection of a cocktail of muscle-specific miRNAs, including miR-206, can accelerate muscle regeneration in a rat injury model (39), although the specific functions of individual miRNAs in this setting were not defined. In this study, we

show that the loss of miR-206 in mice delays muscle regeneration upon CTX injury. Taken together, these results identify miR-206 as an important regulator of muscle regeneration. Analysis of SC differentiation in miR-206–KO mice suggests that miR-206 promotes the differentiation and fusion of progenitor cells into mature myotubes. Thus, the delayed regeneration in miR-206–KO mice upon CTX injury can be attributed to the cell-autonomous function of miR-206 in SC differentiation. Although it is possible that delayed regeneration could also result from an impaired inflammatory response, preventing clearance of damaged myofibers, we do not believe this is the case because miR-206 is only expressed in SCs and not in inflammatory cells (Supplemental Figure 6C).

miR-206 and SC proliferation and differentiation. Our results suggest that miR-206 promotes SC differentiation and represses a set of negative regulators of muscle differentiation, including Pax7, Notch3, and Igfbp5. In the absence of miR-206, SCs show a delay but not a complete block in differentiation, which is likely due to functional redundancy with the closely related miR-1, which is also upregulated upon SC differentiation (25, 27). Pax7 protein is highly expressed in proliferating SCs. Although *Pax7* mRNA levels are upregulated in miR-206–KO SCs under growth conditions, Pax7 protein levels are not significantly changed under these conditions. These findings suggest that additional mechanisms other than miR-206 are responsible for controlling Pax7 protein levels in proliferating SCs. During differentiation, Pax7 is downregulated, and the loss of miR-206 results in attenuation of this downregulation at both mRNA and protein levels. The distinct regulation patterns of Pax7 by miR-206 under growth versus differentiation conditions highlight the notion that the functions of miRNAs are important only under certain cellular phenotypes or conditions.

It was recently reported that miR-206 and miR-133b are encoded by a long noncoding RNA (linc-MD1) (40). linc-MD1 is upregulated in *mdx* mice and promotes muscle differentiation by acting as a competing endogenous RNA (ceRNA) for miR-133 and miR-135 (40). Thus, in addition to regulating SC differentiation through direct binding to the 3′ UTR of target mRNAs, it also possible that miR-206 functions through additional mechanisms to promote the efficient differentiation and fusion of muscle progenitors into myotubes. In this regard, there are several reports of small RNAs being capable of directly activating gene transcription and of miRNAs upregulating the translation of target genes (41, 42).

Our results also indicate that miR-206 does not play a major role in the proliferation of SCs. This is in contrast with a previous study demonstrating that the knockdown of miR-1 and miR-206 in vivo results in an increased rate of proliferation of SCs (25). The discrepancy between our results and those published findings could be because of the inhibition of both miR-1 and miR-206 by antisense oligonucleotides in the published studies. Alternatively, transient inhibition of miR-206 expression in adult mice may have different consequences than genetic deletion throughout life. While genetic deletion and oligonucleotide inhibition of miR-206 lead to different conclusions regarding the role of miR-206 in myoblast proliferation, there are numerous reports that demonstrate a function for miR-206 in promoting the differentiation of muscle progenitors and myoblasts into myotubes (37, 43, 44), as supported by our genetic loss-of-function data.

miR-206 as a modifier of DMD. The *mdx* mouse has provided important insights into the pathological mechanisms of DMD. However, the slow disease progression and mild dystrophic phenotype of *mdx* mice relative to DMD patients have limited the usefulness of this model for therapeutic development. The introduction of secondary gene mutations in *mdx* mice, such as mutations in utrophin, α-dystrobrevin, α7-integrin, or cytidine monophosphate–sialic acid hydroxylase (Cmah) etc., has highlighted the importance of other cellular components in DMD disease progression (45–49). Similarly, genes involved in SC proliferation and differentiation also play regulatory roles in the pathogenesis of *mdx* mice. The severe and rapidly progressing phenotype in *mdx* mice lacking telomerase activity is caused by the reduced regenerative potential of SCs due to shortened telomere length (19). In addition, loss of MyoD in *mdx* mice results in impaired differentiation of SCs, leading to a more severe dystrophic disease phenotype (50). In this report, we show that miR-206 modulates the disease progression of DMD by regulating myogenic differentiation in *mdx* mice.

miR-206 has been shown to be upregulated in *mdx* mice, but it has been unknown whether miR-206 plays a protective or pathogenic role in the disease (24, 27). Our results clearly demonstrate that miR-206 plays a protective role in the setting of muscular dystrophy. The strong activation of miR-206 in *mdx* mice serves as a compensatory mechanism to promote formation of new myofibers in response to injury. In the absence of miR-206, the delayed regeneration and myogenic differentiation result in fibrosis and fatty infiltration as well as mineralization of myofibers, which disrupt muscle integrity and function.

The dramatic worsening of the dystrophic phenotype of *mdx* mice upon genetic deletion of miR-206 is conceptually similar to our prior discovery of the acceleration of skeletal muscle atrophy, paralysis, and death in a mouse model of ALS lacking miR-206 (23). In both cases, strong upregulation of miR-206 expression was seen at disease onset, and miR-206 was found to have a compensatory, protective role in both disease contexts. These 2 studies highlight an important function of miR-206 as a stress-inducible suppressor of skeletal muscle disease. Although we found no innervation defects in miR-206–KO;*mdx* mice compared with *mdx* mice, perhaps the beneficial effects of miR-206 in the 2 disease models point to an unappreciated relationship between muscle SCs and neuromuscular synapse stability.

Therapeutic implications. Since the identification of the dystrophin gene in 1986, there has been intense effort to develop potential therapies for DMD. Current strategies to treat DMD include delivering functional dystrophin via adenoassociated virus vectors, using antisense oligonucleotides to induce exon skipping, allowing production of truncated, but functional, dystrophin protein, or developing stem cell therapies to introduce SCs and myoblasts into muscle (51). Despite advances in these approaches, many challenges remain. The protective role of miR-206 in *mdx* mice raises the possibility that delivery of miR-206 mimics or other strategies to elevate expression of the endogenous *miR-206* gene or modulate its downstream targets could provide therapeutic benefit for DMD or other degenerative skeletal muscle diseases.

Methods

Generation of miR-206–KO;mdx mice. *miR-206*$^{-/-}$ mice in a 129SvEv-C57BL/6 mixed background were described previously (23). *C57BL/10ScSn-Dmd*^{mdx} mice were purchased from the Jackson Laboratory. *miR-206*$^{-/-}$ male mice were bred to homozygous *Dmd*$^{mdx/mdx}$ female mice to generate *miR-206*$^{+/-}$;*Dmd*$^{mdx/+}$ female mice or *miR-206*$^{+/-}$;*Dmd*$^{mdx/Y}$ male mice. *miR-206*$^{+/-}$;*Dmd*$^{mdx/Y}$ male mice were then bred to *Dmd*$^{mdx/mdx}$ female mice to generate *miR-206*$^{+/-}$;*Dmd*$^{mdx/mdx}$ or *miR-206*$^{+/-}$;*Dmd*$^{mdx/Y}$ mice. *miR-206*$^{+/-}$;*Dmd*$^{mdx/mdx}$ female mice

were then intercrossed with *miR-206*$^{+/-}$;*Dmd*$^{mdx/Y}$ male mice to generate *miR-206*$^{-/-}$;*Dmd*$^{mdx/mdx}$ mice and *miR-206*$^{-/-}$;*Dmd*$^{mdx/Y}$ mice, which are referred to as *miR-206–KO;mdx* mice. Mice used in this study were all on a 129SvEv-C57BL/6 mixed background.

CTX injury. CTX from *Naja mossambica mossambica* (Sigma-Aldrich) was dissolved in sterile saline to a final concentration of 10 μM and aliquoted and stored at –20°C. Mice were anesthetized by intraperitoneal injection of 2.5% Avertin at (15 μl/g). Mouse legs were shaved and cleaned with alcohol. TA muscles were injected with 50 μl of CTX with a 26-gauge needle. After injection, animals were kept under a warming lamp until recovery.

Northern blot analysis. Total RNA was isolated from cultured cells by TriZOL (Invitrogen) or from mouse skeletal muscle tissues by the miRNeasy Mini Kit (QIAGEN). Northern blots to detect miR-206, miR-1, and miR-133 and U6 were performed as described previously (52). ^{32}P-labeled Star-Fire oligonucleotide probes (IDT) against mature miRNAs and U6 were used for hybridization.

RT-PCR and real-time RT-PCR analysis. RNA was treated with Turbo RNase-free DNase (Ambion Inc.) prior to the reverse transcription step. RT-PCR was performed using random hexamer primers (Invitrogen). Real-time RT-PCR on miRNA was performed using the TaqMan microRNA assay kits (ABI) according to the manufacturer's protocol. Real-time RT-PCR was performed using TaqMan probes (ABI) or SYBR green probes. SYBR green primers used were as follow: Gja1-F: 5′-GGACCTTGTCCAGCAGCTT-3′, Gja1-R: 5′-TCCAAGGAGTTCCACCACTT-3′; Notch3-F: 5′-AAGC-GTCTCCTGGATGCTG-3′, Notch3-R: 5′-GAATCTGGAAGACACCCTGG-3′; pre-133b-RT-F: 5′CTGGTCAAACGGAACCAAGT-3′, pre-133b-RT-R: 5′-TGATGGCAAAACCAGCATTA-3′.

Microarray analysis. For the microarray, total RNA was isolated from TA muscle of *mdx* and miR-206–KO;*mdx* mice at 3 months of age (n = 3 for each). Microarray analysis was performed by the University of Texas Southwestern Microarray Core Facility using the Mouse Genome Illumina Mouse-6 V2 BeadChip. Data have been deposited in NCBI's Gene Expression Omnibus (GEO GSE36077).

Histological analysis of skeletal muscle. Skeletal muscle groups were harvested and flash frozen in embedding medium containing a 3:1 mixture of Tissue Freezing Medium (Triangle Biomedical Sciences) and gum tragacanth (Sigma-Aldrich) or fixed in 4% paraformaldehyde and processed for routine paraffin histology. Frozen sections were cut on a cryotome and stained with H&E as previously described (53). Masson's trichrome, von Kossa staining, and oil red O staining were performed using standard procedures. Evans blue dye uptake was performed as described (53).

Immunohistochemistry. Frozen sections were fixed in freshly prepared 4% paraformaldehyde for 20 minutes on ice and then treated with 0.3% Triton X-100/PBS at room temperature for 20 minutes. Sections were incubated with mouse IgG-blocking solution from the M.O.M. kit (Vector Lab) diluted in 0.01% Triton X-100/PBS at room temperature for 1 hour. Sections were then incubated with 5% goat serum (Sigma-Aldrich) in M.O.M. protein diluent for 30 minutes. Sections were incubated with primary antibodies diluted in M.O.M. protein diluent at 4°C overnight. The next morning, slides were washed with PBS and incubated with secondary antibodies diluted in M.O.M. protein diluent at room temperature for 45 minutes. Sections were then washed and mounted with VectaShield Mounting Medium with DAPI. Pictures were taken with a Zeiss confocal microscope. Primary and secondary antibodies were as follows: Desmin (1:100, Dako), Laminin (1:200, Sigma-Aldrich), MF20 (DSHB), Pax7 (1:100, DSHB), Alexa Fluor 594 goat anti-mouse IgG1 (1:400, Invitrogen), and Alexa Fluor 488 goat anti-rabbit IgG (1:400, Invitrogen). Wheat germ agglutinin (WGA) staining was performed using Alexa Fluor 555–conjugated WGA (Invitrogen) as previously described (53). Immunostaining of NMJs was done as previously described (23). PECAM1 staining was performed using anti-mouse CD31 antibody (1:40, Dianova) and a biotinylated secondary antibody coupled with streptavidin–horseradish peroxidase, followed by DAB chromagen reaction.

Isolation of SCs by FACS. CTX was injected into hind limb muscles of WT and miR-206–KO mice, and activated SCs were isolated 3 days after injection as previously described (7). Briefly, hind limb muscles were pooled, minced, and digested with 0.2% Collagenase II (Gibco; Invitrogen), followed by trituration. SCs were then isolated by further digestion of myofibers with 0.1% Dispase (Gibco; Invitrogen) and 0.05% Collagenase II (Gibco; Invitrogen). Cell suspension was filtered through a 40-μm cell strainer, and SCs were pelleted after centrifugation.

For FACS, SCs were counted and resuspended in PBS/3% BSA at 1×10^6 cells/50 μl. Cells were then incubated with the following antibodies for 1 hour on ice: Alexa Fluor 488–conjugated rat anti-mouse CD34 (1:50) (AbD Serotec), PE-labeled rat anti-mouse CD45 (1:100), PE-labeled rat anti-mouse CD31 (1:100), PE-labeled anti-mouse Sca-1 (1:3000) (all from BD Biosciences — Pharmingen). After incubation, cells were washed twice, filtered through a 40-μm cell strainer, and resuspended in PBS/3% BSA at a concentration of 2×10^7 cells/ml. Cells were separated on a MoFlo Cytometer (Beckman Coulter). Sorting gates were strictly defined by the forward scatter and side scatter patterns of SCs as well as the positive control cells labeled with Alexa Fluor 488–CD34 and the negative control cells labeled with PE-CD45, PE-CD31, and PE–Sca-1. Cells positive for Alexa Fluor 488–CD34 and negative for PE-CD45, PE-CD31, and PE–Sca-1 were sorted to enrich for activated SCs.

SC cultures. SCs isolated by FACS were cultured on Matrigel-coated (BD Biosciences) plates in growth medium consisting of HAM's F-10 medium, 20% bovine calf serum (BCS), and 5 ng/ml bFGF (Gibco; Invitrogen). Medium was changed daily. Cells were passaged at 70% confluency to prevent spontaneous differentiation. To induce differentiation, cells at 80% confluency were switched to differentiation medium containing DMEM and 2% horse serum.

For immunostaining, cells were grown on Matrigel-coated cover slips in either growth medium or differentiation medium. Cells were fixed on cover slips with 4% paraformaldehyde for 15 minutes, washed with PBS, and permeabilized with 0.3% Triton X-100/PBS for 5 minutes. Cells were blocked with 5% goat serum/PBS/0.1% Triton X-100 for 3 minutes, followed by incubation with primary antibodies (diluted in 5% goat serum/PBS/0.1% Triton X-100) for 2 hours. Cells were then washed in PBS and incubated with secondary antibodies for 1 hour. After washing with PBS, cover slips were mounted on glass slides with VectoLab Mounting Medium (with DAPI). The following antibodies were used: anti-Pax7 (1:100, DSHB), MF20 (DSHB), Alexa Fluor 594 goat anti-mouse IgG1 (for Pax7) (1:400, Invitrogen), and Alexa Fluor 555 goat anti-mouse IgG (for MF20) (1:400, Invitrogen).

Western blot analysis. Total protein was extracted from cultured cells using RIPA buffer containing protease inhibitor cocktail (Roche) and 1 mM PMSF. Protein concentrations were measured by BCA Protein Assay Kit (Thermo Scientific). Equal amounts of protein from different samples were resolved on 4%–20% SDS-PAGE. Western blotting was performed by standard protocol. The following antibodies were used: Pax7 (1:100, DSHB), Notch3 (1:1000, Abcam), IGFBP5 (1:500, Santa Cruz Biotechnology Inc.), connexin43 (1:500, Cell Signaling), and α-tubulin (1:5000, Sigma-Aldrich). For detection of Pax7, HRP-conjugated anti-mouse IgG1 secondary antibody (Santa Cruz Biotechnology Inc.) was used.

Transfection and luciferase assays. 3′ UTR fragments of Notch3, Igfbp5, and Pax7 containing miR-206 binding sites were cloned into pMIR-REPORT Vector (Ambion), respectively. Mutagenesis of the miR-206–binding sites, cell culture, and luciferase assay were performed as previously described (52).

Treadmill test. The treadmill test was performed using the Exer-6M (Columbus Instruments) at 15 degrees downhill. Mice were warmed up at 5 m/min for 5 minutes before the test. For the test, mice ran on the

treadmill at 5 m/min for 2 minutes, 7 m/min for 2 minutes, 8 m/min for 2 minutes, and 10 m/min for 5 minutes. Afterwards, speed was increased 1 m/min to a final speed of 20 m/min. Exhaustion was defined by the inability of the animal to remain on the treadmill despite electrical prodding.

Serum CK measurement. Four-week-old and 5-month-old animals were anesthetized by Avertin, and blood was obtained from the periorbital vascular plexus directly into microhematocrit tubes (70 μl, Fisher Scientific). Serum was obtained by allowing the blood to clot at room temperature for 30 minutes and then centrifuging at 1,700 × *g* for 10 minutes. Serum CK was measured by the University of Texas Southwestern Metabolic Core Facility.

Study approval. All animal experimental procedures were reviewed and approved by the Institutional Animal Care and Use Committees at the University of Texas Southwestern Medical Center at Dallas.

Statistics. Data are presented as mean ± SEM. Differences between groups were tested for statistical significance using the unpaired 2-tailed Student's *t* test. $P < 0.05$ was considered significant.

Acknowledgments

We thank the UT Southwestern Metabolic Phenotype Core Facility for serum CK measurements, and the UT Southwestern Flow Cytometry Core for FACS. We are grateful for assistance from the UT Southwestern Small Animal Imaging Resource, which is supported in part by NCI U24 CA126608, the Harold C. Simmons Cancer Center through an NCI Cancer Center Support Grant, 1P30 CA142543, and the Department of Radiology. We are grateful to the members of the Olson lab for discussions and technical help. We thank Thomas Rando (Stanford University) for the protocols of SC isolation and discussion of the project. We thank Cheryl Nolen and Evelyn Tennison for technical help. We thank Jose Cabrera for graphics and Jennifer Brown for editorial assistance. Work in the laboratory of E.N. Olson was supported by grants from the NIH, the Fondation Leducq, and the Robert A. Welch Foundation (grant number I-0025). N. Liu was supported by a Scientist Development Grant from the American Heart Association.

Received for publication December 30, 2011, and accepted in revised form March 14, 2012.

Address correspondence to: Ning Liu or Eric N. Olson, Department of Molecular Biology, University of Texas Southwestern Medical Center, 5323 Harry Hines Boulevard, Dallas, Texas 75390-9148, USA. Phone: 214.648.1187; Fax: 214.648.1196; E-mail: Ning.Liu@utsouthwestern.edu (N. Liu), Eric.Olson@utsouthwestern.edu (E.N. Olson).

Andrew H. Williams's present address is: Department of Biochemistry and Molecular Biophysics, Columbia University Medical Center, New York, New York, USA.

1. Tedesco FS, Dellavalle A, Diaz-Manera J, Messina G, Cossu G. Repairing skeletal muscle: regenerative potential of skeletal muscle stem cells. *J Clin Invest*. 2010;120(1):11–19.
2. Charge SB, Rudnicki MA. Cellular and molecular regulation of muscle regeneration. *Physiol Rev*. 2004;84(1):209–238.
3. Montarras D, et al. Direct isolation of satellite cells for skeletal muscle regeneration. *Science*. 2005; 309(5743):2064–2067.
4. Collins CA, et al. Stem cell function, self-renewal, and behavioral heterogeneity of cells from the adult muscle satellite cell niche. *Cell*. 2005;122(2):289–301.
5. Kuang S, Kuroda K, Le Grand F, Rudnicki MA. Asymmetric self-renewal and commitment of satellite stem cells in muscle. *Cell*. 2007;129(5):999–1010.
6. Sherwood RI, et al. Isolation of adult mouse myogenic progenitors: functional heterogeneity of cells within and engrafting skeletal muscle. *Cell*. 2004; 119(4):543–554.
7. Conboy IM, Conboy MJ, Smythe GM, Rando TA. Notch-mediated restoration of regenerative potential to aged muscle. *Science*. 2003;302(5650):1575–1577.
8. Seale P, Sabourin LA, Girgis-Gabardo A, Mansouri A, Gruss P, Rudnicki MA. Pax7 is required for the specification of myogenic satellite cells. *Cell*. 2000; 102(6):777–786.
9. Kuang S, Gillespie MA, Rudnicki MA. Niche regulation of muscle satellite cell self-renewal and differentiation. *Cell Stem Cell*. 2008;2(1):22–31.
10. Lepper C, Partridge TA, Fan CM. An absolute requirement for Pax7-positive satellite cells in acute injury-induced skeletal muscle regeneration. *Development*. 2011;138(17):3639–3646.
11. Sambasivan R, et al. Pax7-expressing satellite cells are indispensable for adult skeletal muscle regeneration. *Development*. 2011;138(17):3647–3656.
12. Murphy MM, Lawson JA, Mathew SJ, Hutcheson DA, Kardon G. Satellite cells, connective tissue fibroblasts and their interactions are crucial for muscle regeneration. *Development*. 2011; 138(17):3625–3637.
13. McCarthy JJ, et al. Effective fiber hypertrophy in satellite cell-depleted skeletal muscle. *Development*. 2011;138(17):3657–3666.
14. Hoffman EP, Brown RH Jr, Kunkel LM. Dystrophin: the protein product of the Duchenne muscular dystrophy locus. *Cell*. 1987;51(6):919–928.
15. Chamberlain JS, et al. Expression of the murine Duchenne muscular dystrophy gene in muscle and brain. *Science*. 1988;239(4846):1416–1418.
16. Wallace GQ, McNally EM. Mechanisms of muscle degeneration, regeneration, and repair in the muscular dystrophies. *Annu Rev Physiol*. 2009;71:37–57.
17. McNally EM, Pytel P. Muscle diseases: the muscular dystrophies. *Annu Rev Physiol*. 2007;2:87–109.
18. Chamberlain JS, Banks GB. The value of mammalian models for Duchenne muscular dystrophy in developing therapeutic strategies. *Curr Top Dev Biol*. 2008; 84:431–453.
19. Sacco A, et al. Short telomeres and stem cell exhaustion model Duchenne muscular dystrophy in mdx/mTR mice. *Cell*. 2010;143(7):1059–1071.
20. Bartel DP. MicroRNAs: genomics, biogenesis, mechanism, and function. *Cell*. 2004;116(2):281–297.
21. Eisenberg I, Alexander MS, Kunkel LM. miRNAS in normal and diseased skeletal muscle. *J Cell Mol Med*. 2009;13(1):2–11.
22. Williams AH, Liu N, van Rooij E, Olson EN. MicroRNA control of muscle development and disease. *Curr Opin Cell Biol*. 2009;21(3):461–469.
23. Williams AH, et al. MicroRNA-206 delays ALS progression and promotes regeneration of neuromuscular synapses in mice. *Science*. 2009; 326(5959):1549–1554.
24. Yuasa K, Hagiwara Y, Ando M, Nakamura A, Takeda S, Hijikata T. MicroRNA-206 is highly expressed in newly formed muscle fibers: implications regarding potential for muscle regeneration and maturation in muscular dystrophy. *Cell Struct Funct*. 2008;33(2):163–169.
25. Chen JF, et al. microRNA-1 and microRNA-206 regulate skeletal muscle satellite cell proliferation and differentiation by repressing Pax7. *J Cell Biol*. 2010; 190(5):867–879.
26. Liu N, Olson EN. MicroRNA regulatory networks in cardiovascular development. *Dev Cell*. 2010; 18(4):510–525.
27. Cacchiarelli D, et al. MicroRNAs involved in molecular circuitries relevant for the Duchenne muscular dystrophy pathogenesis are controlled by the dystrophin/nNOS pathway. *Cell Metab*. 2010; 12(4):341–351.
28. Goebel HH. Desmin-related neuromuscular disorders. *Muscle Nerve*. 1995;18(11):1306–1320.
29. Helliwell TR. Lectin binding and desmin staining during bupivicaine-induced necrosis and regeneration in rat skeletal muscle. *J Pathol*. 1988; 155(4):317–326.
30. Zatz M, et al. Serum creatine-kinase (CK) and pyruvate-kinase (PK) activities in Duchenne (DMD) as compared with Becker (BMD) muscular dystrophy. *J Neurol Sci*. 1991;102(2):190–196.
31. Lyons PR, Slater CR. Structure and function of the neuromuscular junction in young adult mdx mice. *J Neurocytol*. 1991;20(12):969–981.
32. Fox MA, et al. Distinct target-derived signals organize formation, maturation, and maintenance of motor nerve terminals. *Cell*. 2007;129(1):179–193.
33. Beres BJ, et al. Numb regulates Notch1, but not Notch3, during myogenesis. *Mech Dev*. 2011; 128(5–6):247–257.
34. Cobb LJ, et al. Partitioning of IGFBP-5 actions in myogenesis: IGF-independent anti-apoptotic function. *J Cell Sci*. 2004;117(pt 9):1737–1746.
35. Salih DA, et al. Insulin-like growth factor-binding protein 5 (Igfbp5) compromises survival, growth, muscle development, and fertility in mice. *Proc Natl Acad Sci U S A*. 2004;101(12):4314–4319.
36. James PL, Stewart CE, Rotwein P. Insulin-like growth factor binding protein-5 modulates muscle differentiation through an insulin-like growth factor-dependent mechanism. *J Cell Biol*. 1996; 133(3):683–693.
37. Kim HK, Lee YS, Sivaprasad U, Malhotra A, Dutta A. Muscle-specific microRNA miR-206 promotes muscle differentiation. *J Cell Biol*. 2006; 174(5):677–687.
38. Rao PK, Kumar RM, Farkhondeh M, Baskerville S, Lodish HF. Myogenic factors that regulate expression of muscle-specific microRNAs. *Proc Natl Acad Sci U S A*. 2006;103(23):8721–8726.
39. Nakasa T, Ishikawa M, Shi M, Shibuya H, Adachi N, Ochi M. Acceleration of muscle regeneration by local injection of muscle-specific microRNAs in rat skeletal muscle injury model. *J Cell Mol Med*. 2010;14(10):2495–2505.
40. Cesana M, et al. A long noncoding RNA controls

muscle differentiation by functioning as a competing endogenous RNA. *Cell*. 2011;147(2):358–369.
41. Schwartz JC, et al. Antisense transcripts are targets for activating small RNAs. *Nat Struct Mol Biol*. 2008;15(8):842–848.
42. Vasudevan S, Tong Y, Steitz JA. Switching from repression to activation: microRNAs can up-regulate translation. *Science*. 2007;318(5858):1931–1934.
43. Dey BK, Gagan J, Dutta A. miR-206 and -486 induce myoblast differentiation by downregulating Pax7. *Mol Cell Biol*. 2011;31(1):203–214.
44. Zhang W, Wang T, Su Y, Li W, Frame LT, Ai G. Recombinant adenoviral microRNA-206 induces myogenesis in C2C12 cells. *Med Sci Monit*. 2011; 17(12):BR364–BR371.
45. Deconinck AE, et al. Utrophin-dystrophin-deficient mice as a model for Duchenne muscular dystrophy. *Cell*. 1997;90(4):717–727.
46. Grady RM, Teng H, Nichol MC, Cunningham JC, Wilkinson RS, Sanes JR. Skeletal and cardiac myopathies in mice lacking utrophin and dystrophin: a model for Duchenne muscular dystrophy. *Cell*. 1997;90(4):729–738.
47. Grady RM, et al. Role for alpha-dystrobrevin in the pathogenesis of dystrophin-dependent muscular dystrophies. *Nat Cell Biol*. 1999;1(4):215–220.
48. Guo C, et al. Absence of alpha 7 integrin in dystrophin-deficient mice causes a myopathy similar to Duchenne muscular dystrophy. *Hum Mol Genet*. 2006; 15(6):989–998.
49. Chandrasekharan K, et al. A human-specific deletion in mouse Cmah increases disease severity in the mdx model of Duchenne muscular dystrophy. *Sci Transl Med*. 2010;2(42):42ra54.
50. Megeney LA, Kablar B, Garrett K, Anderson JE, Rudnicki MA. MyoD is required for myogenic stem cell function in adult skeletal muscle. *Gene Dev*. 1996;10(10):1173–1183.
51. Muntoni F, Wood MJ. Targeting RNA to treat neuromuscular disease. *Nat Rev Drug Discov*. 2011; 10(8):621–637.
52. Liu N, et al. microRNA-133a regulates cardiomyocyte proliferation and suppresses smooth muscle gene expression in the heart. *Gene Dev*. 2008; 22(23):3242–3254.
53. Liu N, et al. Mice lacking microRNA 133a develop dynamin 2-dependent centronuclear myopathy. *J Clin Invest*. 2011;121(8):3258–3268.